Direct numerical simulations of hypersonic boundary layer transition control via non-uniform surface temperature distribution

Luca Boscagli*[a], Olaf Marxen†[b], Georgios Rigas‡[a], and Paul Bruce§[a]
[a]*Imperial College London, London, UK, SW7 2AZ*
[b]*University of Surrey, Guildford, UK, GU2 7XH*

The notable heat fluxes that characterize hypersonic flows significantly limit the flight envelope and performance of hypersonic vehicles. The role of hydrodynamic instability and the onset of laminar to turbulent boundary layer transition is important, and several control methods have been attempted and reported in the literature. The effect of streaks on the suppression of two dimensional (second Mack mode) instabilities has been numerically and experimentally investigated, but a robust control method has not yet been established. Previous work has shown that streaks can be generated through a spanwise variation in surface temperature. This method exploits the aerothermodynamic characteristics of the flow, and promises to be robust and highly tuneable. This work uses time-dependent, compressible direct numerical simulations to determine and quantify the effectiveness of this novel control method in the suppression and delay of second Mack mode instability and laminar to turbulent transition for a Mach 6 hypersonic boundary layer over a flat plate. The effect of streak wavelength on stabilization performance is determined; a near-optimum condition is achieved for streaks with a wavelength approximately 8 to 10 times the local boundary layer thickness. The effect of the non-uniform surface temperature on laminar to turbulence transition via second Mack mode fundamental resonance is also investigated. It is shown that the control method is able to reduce the amplitude of high-frequency (second Mack mode related) peak shear-stresses by approximately 30%, and delay transition. Upon further numerical and experimental investigations, the control method promises an increase in the aero-thermal-structural efficiency of future hypersonic technologies.

I. Nomenclature

A_{T_w}	=	non-dimensional amplitude of surface temperature variation
$\alpha = \alpha_r + i\alpha_i$	=	streamwise wavenumber and growth rate ($\in \mathbb{C}$)
$\beta = \beta_r$	=	spanwise wavenumber for the linear stability theory notation($\in \mathbb{R}$)
C_f	=	skin friction coefficient
c_{ph}	=	phase speed
δ_{99}	=	boundary layer thickness
f, k	=	frequency and spanwise wavenumber for the DNS notation
F	=	non-dimensional frequency of the linear perturbation
λ_z	=	spanwise extent of the computational domain
L_y,	=	computational domain height
M_∞,	=	freestream Mach number
Pr	=	Prandtl number
Re	=	Reynolds number
T_w	=	non-dimensional wall temperature
T_∞	=	freestream static temperature
ν	=	kinematic viscosity

*Research Associate, Department of Aeronautics, l.boscagli@imperial.ac.uk
†Senior Lecturer, School of Mechanical Engineering Sciences
‡Reader, Department of Aeronautics
§Reader, Department of Aeronautics, AIAA Associate Fellow

U, V, W	=	non-dimensional streamwise, wall-normal and spanwise velocity components
$x_{bs,s}, x_{bs,e}$	=	streamwise locations corresponding to the start and end of the blowing-suction region
x, y, z	=	non-dimensional streamwise, wall-normal and spanwise coordinates
ω	=	angular frequency ($\in \mathbb{R}$)

II. Introduction

In recent years, there is increasing interest in further development of aerospace technologies for dual use applications that can travel at hypersonic speeds. At such high flight speeds, a complex aerothermodynamic behaviour challenges the performance of any vehicle that operates under this flight regime. Notable aerodynamic heating of the external surface and viscous drag increase can significantly limit the flight envelope and operability of hypersonic vehicles.

The role of laminar to turbulent boundary layer transition on the aerothermodynamic characteristics of the flow on the external surface of hypersonic vehicles is known to represent one of the key design drivers. Several attempts have been made to control the streamwise location of the transition onset to achieve performance benefits. For a flight Mach number (M_∞) approximately above 4 and below 6, and for a thermally insulated (adiabatic) wall, or under thermal equilibrium conditions (radiative-adiabatic, [1]), an important boundary layer instability mechanism is known to be two dimensional and dominated by high-frequency ($[10^5, 10^6]$Hz, [2]) acoustic waves trapped between the wall and the relative sonic line within the boundary layer [3]. This instability mechanism is typically referred to as second Mack mode instability. The high-frequency dilatation work of the second Mack mode instability on the flow can also lead to significant local aerodynamic heating [4], which can further reduce the aero-thermal efficiency of hypersonic vehicles.

For thermally insulated conical bodies, Paredes et al. [5] numerically showed, through the non-parallel, Parabolized Stability Equations (PSE), that it is possible to stabilize the second Mack mode through the generation of spatially coherent flow structures (streaks), which travel at a lower (or higher) velocity relative to the mean, undisturbed flow within the boundary layer. For a flight Mach number above 4, the generation of streaks was beneficial to delay the onset of laminar to turbulent transition, and therefore to potentially reduce the viscous drag and aerodynamic surface heating. Paredes et al. [5] also showed that the theoretical benefits achievable by delaying the second Mack mode may be limited by potential adverse effects of the streaks on three dimensional non-inflectional instability mechanisms (first Mack mode). This is particularly true at lower Mach numbers ($M_\infty = 3$), where, for an adiabatic flat plate configuration [6], the interaction between the streaks sub-harmonics and the first Mack mode can lead to earlier transition to turbulence in quiet, low external disturbance, environments. For a lower Mach number ($M_\infty = 2$) boundary layer over an adiabatic flat plate, Sharma et al. [7] and Kneer et al. [8] conducted a set of parametric DNS studies and showed that streaks generated by a blowing and suction strip can successfully delay first mode oblique breakdown to turbulence. For a similar configuration, Celep et al. [9] showed that uniform wall heating can reduce the useful range of control-streak amplitude that can successfully delay transition. For $M_\infty = 4.5$, Zhou et al. [10] showed that second mode oblique breakdown can also be successfully delayed through finite amplitude streaks. For low-speed flows, Andersson et al. [11] showed that streaks can impart a spatial organization to the supported instabilities, which manifests in the symmetric (varicose-type) or asymmetric (sinuous-type) characteristics of the eigenfunction of the instability mode relative to the streak structure. In compressible boundary layers, steady streaks typically undergo significant transient (non-modal) temporal [12] and spatial [13] growth. Based upon this evidence, Caillaud et al. [14] investigated through linearized Direct Numerical Simulations (DNS) the dynamics of non-modal instability for a hypersonic boundary layer ($M_\infty = 6$) over an adiabatic flat plate with streaks generated through a volumetric momentum force. Several interaction mechanisms were determined based on the amplitude of the forcing streaks ($As_{u,0}$). For $As_{u,0} = 0.028$, the associated maximum amplitude of the streaks at the end of the domain was $As_u \approx 0.4$ and the symmetric, fundamental and first sub-harmonic second Mack mode were destabilized by the streaky flow.

Passive control of hypersonic boundary layer transition has been experimentally and numerically attempted through the use of roughness elements [15–17] or vortex generators [18]. Marxen et al. [15] used high-order compressible DNS computations to investigate the growth rate of convective disturbances within a boundary layer at $M_\infty = 4.8$ with two dimensional roughness elements. For high-frequency (second Mack mode type) disturbances, the spatial damping effect of the two dimensional, localized, roughness elements was significant. For a similar geometry configuration and for $M_\infty = 5.92$, Duan et al. [19] showed that the streamwise position of the roughness element is an important factor in the control of two and three dimensional (oblique) instabilities. For a cone configuration, Fong et al. [16] showed that if the streamwise locations of the roughness elements is informed by numerical (linear) analysis of the boundary layer stability, it is possible to achieve stabilization of both first and second Mack modes. However, these passive control devices present several implementation challenges at hypersonic speeds. Under the cruise segment of flight, due to the long

exposure to high heat flux these elements can be melted down or their aerodynamic shape deformed in such a way that the potential transition benefits may be completely eroded. Similarly, under off-design conditions, these devices may represent an additional source of viscous and pressure drag that can limit the manoeuverability of the vehicle. Thus, novel robust control methods are required for hypersonic regimes. Recent computational [20] and experimental [21] studies showed that for a flat plate configuration it is possible to generate streaks within the boundary layer through a spanwise non-uniform wall temperature distribution. This can be passively attained through the use of alternate stripes of materials with different thermal properties, and by exploiting the high heat flux characteristics of the hypersonic regime. This non-intrusive, passive flow control technique has the potential to increase the aero-thermal-structural efficiency of hypersonic vehicles. However, there is a need to determine its effectiveness and limits on both second Mack mode stabilization and transition delay.

The aim of this work is to assess, via Direct Numerical Simulations (DNS), the effect of streaks generated through non-uniform surface temperature distributions on boundary layer instability and transition to turbulence. Section III presents the case study, computational domain and numerical methods used. Results and discussion are presented in sections IV and V. Firstly, the evolution and amplification of small amplitude disturbances in the computational domain is investigated and the effect of the novel control method on second Mack mode stabilization is presented. Secondly, the effect on laminar to turbulent transition under deterministic forcing is determined and quantified. Finally, a summary of the impact and contribution of this work is presented in section VI.

III. Methodology

The development of instabilities and transition to turbulence of a high-speed boundary layer over a flat plate with uniform and non-uniform surface temperature distributions is investigated by means of 3D Direct Numerical Simulations (DNS). Linear Stability Theory (LST) analysis is used to inform the selection of some of the boundary conditions for the DNS computations. In the sections below a brief description of the numerical methods and notation, and the formulation of the wall boundary conditions used is provided.

A. Direct numerical simulations

The computational domain for the DNS (Fig. 1) includes the viscous wall, where a laminar self-similar solution develops, and inflow, outflow and upper boundaries, where sponge regions are used to damp the solution towards a self-similar laminar state and prevent spurious reflection of pressure waves (Fig. 1a). Periodic boundary conditions are applied in the spanwise direction at both sides of the domain (Fig. 1b).

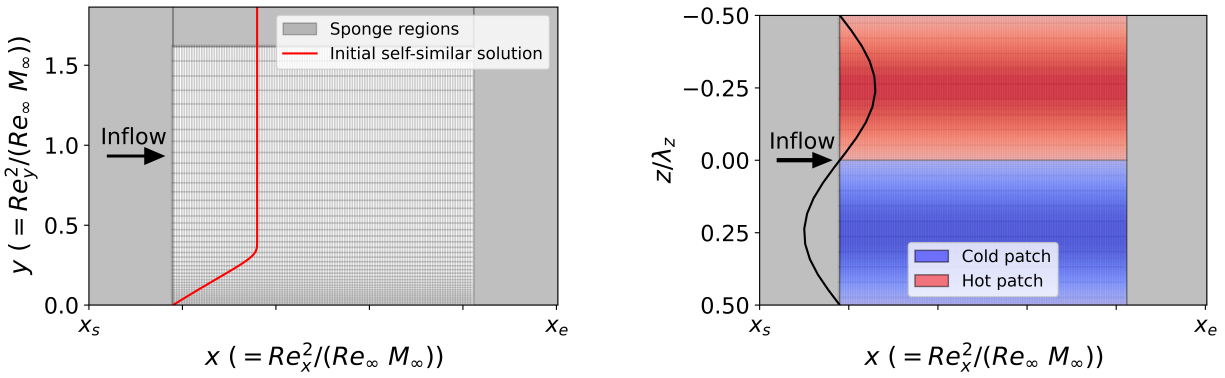

(a) **(b)**

Fig. 1 (a) Streamwise, x, and (b) spanwise, z, 2D schematics of the computational domain, boundary conditions and initial solution. Streamwise and wall-normal, y, grid refinement displayed every 10^{th} and 5^{th} point, respectively. Flow is left to right, and the domain is periodic in the spanwise direction.

The three dimensional, time-dependent, compressible formulation of the Navier Stokes equations is solved for a calorically perfect gas (air). For the same working fluid and for a range of freestream specific total enthalpies similar to the one investigated in this work, Bitter and Shepherd [22] showed that, as the ratio of diffusion to reaction timescales

was close to one, the effect of thermal non-equilibrium on maximum spatial growth rate for the second Mack mode was less than 8%, and it did not affect the dominant aerodynamic mechanisms of the boundary layer instability. Thus, the thermochemical equilibrium assumption is sufficiently valid within the context of this work. A non-dimensional form of the conservative variables is used, and the non-dimensionalization is mostly based on the free-stream conditions [15]. In the following, the dimensional variables are marked with the symbol $\tilde{(\cdot)}$, whereas the latter is omitted for the non-dimensional form. Sutherland's law, with Sutherland's temperature $\tilde{T}_s = 110.4$K [1], is used to compute viscosity. From the used non-dimensionalization of the Navier-Stokes equations, the Reynolds number (Re_∞) and Prandtl number (Pr_∞) formulation is as follows,

$$Re_\infty = \tilde{\rho}_\infty \tilde{c}_\infty \tilde{L}_{ref} / \tilde{\mu}_\infty \tag{1}$$

$$Pr_\infty = \tilde{\mu}_\infty \tilde{c}_p / \tilde{k}_\infty, \tag{2}$$

where $\tilde{\rho}_\infty$, $\tilde{c}_\infty$, $\tilde{\mu}_\infty$ and $\tilde{k}_\infty$ are the freestream density, speed of sound, dynamic viscosity and thermal conductivity, respectively, $\tilde{L}_{ref}$ is the reference lengthscale, and $\tilde{c}_p$ is the specific heat at constant pressure. In all the figures below, velocity and temperature scales are normalized with the freestream velocity, $\tilde{u}_\infty$, and static temperature, $\tilde{T}_\infty$, respectively. In place of the non-dimensional streamwise coordinate, x, a local Reynolds number, $Re_x = \sqrt{x Re_\infty M_\infty}$, is sometimes also used. The ratio of the specific heats (γ) is set to $\gamma = 1.4$, and $Pr_\infty = 0.71$.

The equations are discretized on a spatially structured, curvilinear grid with a staggered approach for the conservative variables, and a time-accurate solution is achieved through a 6^{th} order compact finite difference scheme within the interior nodes of the domain and with an explicit 3^{rd} order Runge-Kutta time-stepping method [15, 23, 24]. Relative to the computations with small amplitude disturbances, the streamwise direction is discretized with 1200 nodes, which approximately corresponds to 22 points per second Mack mode streamwise wavelength. Based on previous studies [25], this guarantees sufficiently grid independent results for an adiabatic flat plate. In the wall-normal direction 211 nodes are used with grid stretching [15] near the wall (Fig. 1a), such that for each of the computations the boundary layer is resolved with at least 85 points. In the spanwise direction 13 points per spanwise wavelength of the streaks (λ_z) are used. Based on a grid independence studies (section A), this provides sufficient spanwise resolution for the assessment of amplification of small amplitude disturbances with streaks. For time-accuracy, the second Mack mode fundamental period ($\tau_0 = 2\pi/\omega_0$) is resolved with 600 timesteps. The selection of angular frequency (ω_0) to trigger second Mack mode instability via blowing and suction within the domain is further described in the following section (section III.A.1). The choice of the computational timestep is based on previous studies [15] and it guarantees sufficient temporal resolution to capture the second Mack mode instabilities.

1. Blowing and suction boundary condition

To trigger boundary layer instabilities and promote transition to turbulence, a wall-normal momentum perturbation is introduced downstream of the domain inflow and upstream of the region of interest. The formulation (Eq. 3) is similar to that used by Pagella et al. [26] and Marxen et al. [15],

$$\begin{cases} \frac{(\tilde{\rho}\tilde{v})_{wall}}{(\tilde{\rho}\tilde{c})_\infty} = (\rho v)_{wall} = A_v \sin(\omega t) \sin(n\xi) \exp(-\epsilon\xi^2) \\ \xi = \frac{x - x_{c,strip}}{L_{strip}} \end{cases} \tag{3}$$

For a more concise notation, in the rest of the text, this boundary condition is referred to as actuator. The streamwise location of the center of the actuator ($x_{c,strip}$) and its length (L_{strip}) are determined based on linear stability analyses as described in section III.B. The amplitude of the perturbation introduced by the actuator (A_v) is set to $A_v = 0.0006 M_\infty$. This choice is based on previous studies in the literature [27, 28], and it is sufficiently small to avoid bypass of the linear instability regime. For the transition to turbulence studies, the actuator law and the disturbances amplitude are varied as described in section V.A. In equation 3, the parameters n and ζ control the number of actuators used to trigger the instability and the spatial damping of A_v. A preliminary assessment showed that $n = 4$ provides a sufficiently computationally efficient way to trigger boundary layer instability, and
$epsilon = \sqrt{2}/2$ was selected based on previous work [26].

2. Wall temperature boundary condition

The wall temperature boundary condition is

$$T_w = T_{w,base}\left(1 + A_{T_w}\sin\left(\frac{2\pi}{\lambda_z}z\right)\right) \tag{4}$$

where A_{T_w} sets the amplitude of the wall temperature variation relative to the baseline (uniform) wall temperature. The wall temperature is imposed as a modification to the internal energy, which is specified within the fluid region at the cell-center, and a five-cell stencil linear interpolation is used to get the value at the boundaries (the wall). A linear temporal ramp-up of A_{T_w} is used as part of the convergence strategy. Within that period, data are discarded as part of the initial numerical transient and not taken into account within the analysis.

B. Linear stability theory

Local, parallel Linear Stability Theory (LST) analysis is used to inform the selection of the computational domain size ($[x_s, x_e]$, Fig. 1a) for the DNS, as well as the choice of the forcing frequency and size of the blowing and suction region used to trigger boundary layer instabilities. The ansatz formulation for the solution of the linearized Navier Stokes equations (q') is expressed as follows,

$$q'(x, y, z; t) = \hat{q}(y)e^{i(\alpha x+\beta z-\omega t)} \tag{5}$$

where α and β are the streamwise and spanwise wavenumbers, respectively, ω is the angular frequency and $\hat{q}$ is the wall normal distribution of the eigenfunction. Further details about the numerical implementation of the LST code can be found in Mack (1976) [29]. The LST is used within a spatial framework, and therefore α is complex, while β and ω are real numbers. The spatial growth rate is expressed by α_i and the laminar boundary layer is linearly unstable for $-\alpha_i > 0$. The LST results presented in this work were benchmarked with existing data in the literature. For $M_\infty > 4$, the difference in the spatial growth rate for the second Mack mode was below 10% (further details are in appendix B). The agreement is deemed satisfactory for the purpose of this work, which is focused on the assessment, via DNS, of the effect of non-uniform surface temperature distribution on the instability and transition of a hypersonic boundary layer.

C. Data analysis methods

The computations are advanced in time for about 250 to 300 times the fundamental period ($\tau_0 = 2\pi/\omega_0$). An initial numerical transient is discarded to allow the initial pressure disturbance due to the actuator to be convected outside the domain, and for the amplitude of sub-harmonic of the disturbance forcing frequency to decay. Data are collected at a sampling rate $300/\tau_0$ for approximately $10\tau_0$, which provides sufficient spectral resolutions and statistical convergence of the growth rate. The spanwise homogeneity of the flow is exploited for frequency (f) and spanwise wavenumber (k) Fourier decomposition. For the small amplitude disturbances studies, streaks, second Mack mode and non-linear interactions are indicated with $(f, k) = (0, 1)$, $(1, 0)$ and $(1, 1)$, respectively. A slight change in notation is introduced for the transition to turbulence studies as further described in section V.A to reflect the changes in the actuator law of the forcing disturbances and spanwise extent of the computational domain relative to the streaks' wavelength. The modal energy is computed based on Chu's energy (E^{fk}_{Chu}, eq. 6) [30] as follows.

$$E^{fk}_{Chu}(x) = \frac{1}{2}\int_0^{L_y}\left[\overline{\rho}\left(\hat{u}'\hat{u}'^* + \hat{v}'\hat{v}'^* + \hat{w}'\hat{w}'^*\right) + \frac{\overline{T}}{\gamma M^2_\infty \overline{\rho}}\hat{\rho}'\hat{\rho}'^* + \frac{\overline{\rho}}{\gamma\left(\gamma-1\right)M^2_\infty \overline{T}}\hat{T}'\hat{T}'^*\right]dy \tag{6}$$

where $\overline{(\cdot)}$, $(\cdot)'$ and $\hat{(\cdot)}$ indicate the mean flow deformation, fluctuations and the Fourier coefficient, respectively, and $(\cdot)^*$ indicates the complex conjugate. L_y indicates the wall-normal extent of the computational domain. The streamwise evolution of the streaks amplitude ($As_u(x)$, eq. 7) is computed as,

$$As_u(x) = \frac{1}{2}\left[\max_{y,z}\left(U(x) - \overline{U}(x)\right) - \min_{y,z}\left(U(x) - \overline{U}(x)\right)\right] \tag{7}$$

The definition was initially introduced for low speed flows by Andersson et al. [11], and adopted in most of the recent literature for supersonic and hypersonic flows [14, 18].

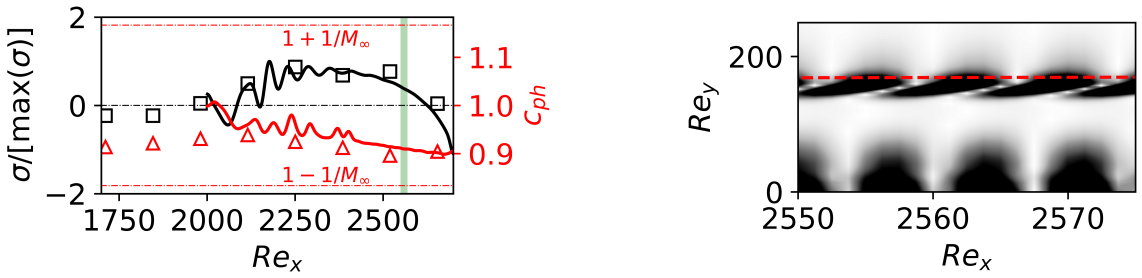

(a) **(b)**

Fig. 2 (*a*) Second Mack mode growth rate (σ, black) and non-dimensional phase speed (c_{ph}, red) based on DNS (lines) and LST (markers); DNS data computed from wall static pressure fluctuations. Black dashed line demarcates second Mack mode stable ($\sigma < 0$) and unstable($\sigma > 0$) regions, respectively; red dashed lines mark the phase speed of slow ($1 - 1/M_\infty$) and fast acoustic waves ($1 + 1/M_\infty$); the green shaded region marks the streamwise extent of the plot in (*b*). (*b*) DNS time snapshot of streamwise density gradient fluctuations; red dashed line: $u = 0.999$. Uniform ($T_w = 3$) case.

IV. Evolution of small amplitude disturbances

In the following sections, DNS studies are presented to assess the effect of streaks generated through spanwise non-uniform surface temperature distribution on the second Mack mode linear amplification. The operating conditions are based upon previous work [20], and these are $M_\infty = 6$, $\tilde{T}_{w,\infty} = 216.7$K and unit Reynolds number based on the free stream speed $Re_{unit} \approx 11 \times 10^6$1/m. The effect of uniform heating and cooling on second Mack mode is verified via both DNS and LST analyses. The effect of spanwise wavelength of the control-streaks on the effectiveness of the control method is determined and quantified.

A. Baseline configuration with uniform surface temperature

A cold flat plate is used as a baseline (uncontrolled) case, with $T_w = T_{w,base} = 3$, which corresponds to approximately 42% of the adiabatic wall temperature (T_{aw}) and it is sufficiently representative of flight conditions [31]. For this case, the maximum growth rate (σ) of the second Mack mode occurs at approximately $Re_x \approx 2500$ (figure 2a), and it manifests with a typical phase speed $c_{ph} \approx 0.9$, and rope-like signature in the fluctuations of the streamwise density gradient (figure 2b). The agreement between LST and DNS (figure 2a) confirms the appropriate selection of the time-space characteristics of the wall-normal momentum perturbation to trigger the second Mack mode.

1. Effect of uniform heating and cooling

To further verify that the second Mack mode instability is successfully triggered within the DNS domain, the wall temperature is uniformly increased ($T_w = 4$) and decreased ($T_w = 2$) relative to the baseline computation (figure 3a) and the DNS results are compared with the LST results. For this case study, the growth rate of the instability (σ) in the DNS is computed based on the spanwise averaged wall static pressure fluctuations and the results are normalized relative to the maximum growth rate for the baseline case (max $\left(\sigma_{T_w=3}\right)$). As expected based on previous research [3], cooling and heating destabilizes and stabilizes the second Mack mode, respectively (figure 3b). Both DNS and LST are able to capture these effects, and this provides confidence that second Mack mode instability is triggered in the DNS computations, despite some differences in the decay rate between LST and DNS.

B. Effect of spanwise non-uniform surface temperature

For the controlled configuration, the amplitude of the spanwise temperature variation is set to $A_{T_w} = 0.3$ for both the hot and cold patch, such that a left/right symmetric configuration is investigated, and the base flow surface temperature for both the controlled and uncontrolled case is the same ($T_{w,base} = 3$). For the controlled case, the maximum ($T_w = 4$) and minimum ($T_w = 2$) wall temperature is approximately 58% and 29% the adiabatic wall temperature, respectively. For this assessment, the spanwise wavelength of the streaks ($\lambda_{z,s}$) corresponds to the spanwise extent of the computational domain (λ_z) and for the initial case study $\lambda_z = 1.2$. Both the controlled and the

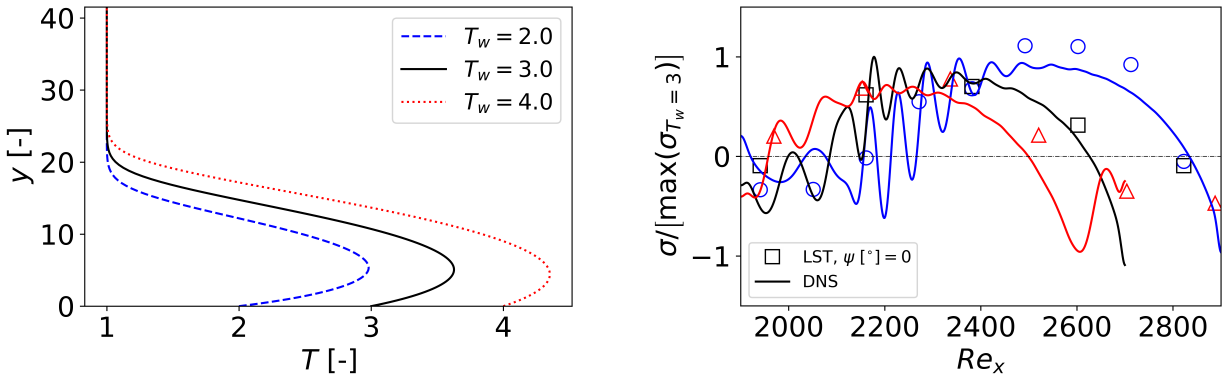

(a) (b)

Fig. 3 (*a*) Self-similar temperature profiles and (*b*) second Mack mode growth rate based on DNS (lines) and LST (markers). In (*b*), the DNS data are computed from the spanwise averaged wall static pressure fluctuations; the black dashed line demarcates second Mack mode stable ($\sigma < 0$) and unstable($\sigma > 0$) regions, respectively

uncontrolled configurations are initialized with a self-similar laminar solution for an isothermal flat plate boundary layer corresponding to the uncontrolled (uniform) baseline wall temperature, $T_{w,base} = 3$. The amplitude (As_u,[11]) of the control-streaks undergoes a noticeable growth from the start of the non-uniform wall temperature distribution to the end of the computational domain (Fig. 4a). The manipulation of the surface temperature distribution (Fig. 4b) to generate streaks leads to spanwise asymmetry in the flow for the controlled case (Fig. 4c). This is mostly driven by the different effect of heating and cooling on second Mack mode [3]. The control-streaks reduce the modal energy associated to the second Mack mode (Fig. 5), which is stabilized by the spanwise non-uniform surface temperature distribution.

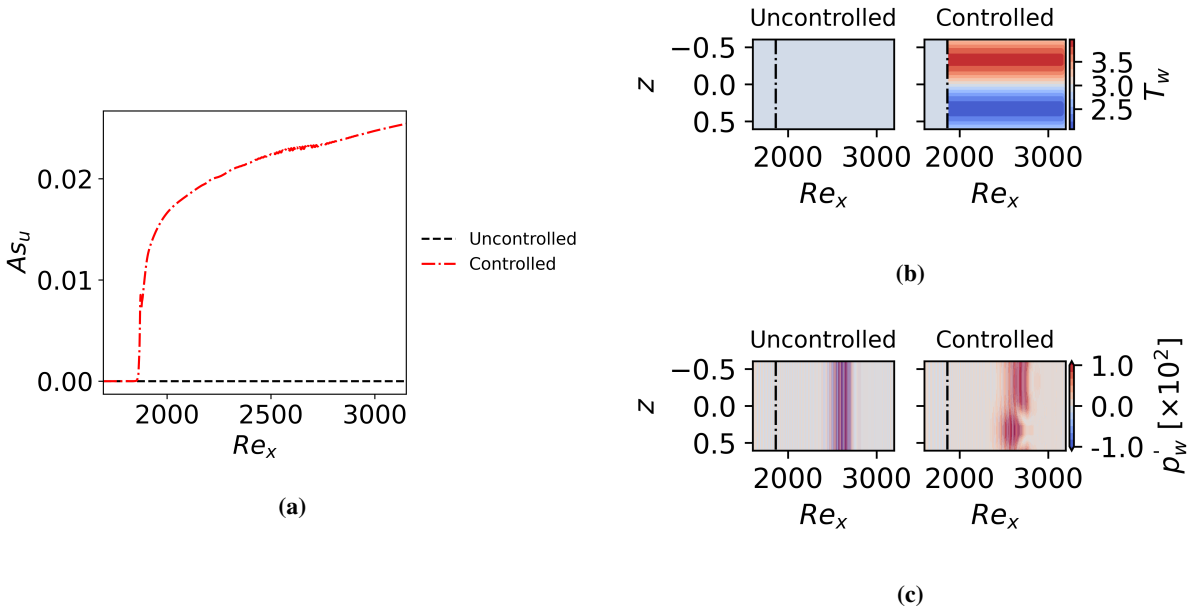

(a) (b) (c)

Fig. 4 Effect of control method on (*a*) streamwise distribution of streaks amplitude, (*b*) wall temperature distribution and (*c*) instantaneous, non-dimensional wall static pressure fluctuations (p'_w). In (*b*) and (*c*) the black dot-dashed line marks the end of the actuator region.

The inset in figure 5 depicts the modal energy associated to the forcing disturbance, which is the same for the controlled and uncontrolled configurations. Thus, the stabilization of the second Mack mode due to the spanwise

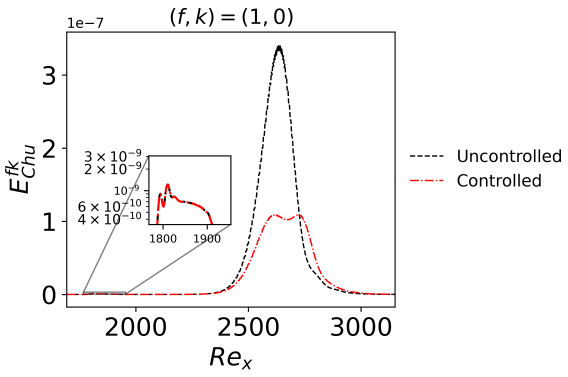

Fig. 5 Effect of control method on second Mack mode modal energy.

non-uniform surface temperature is quantified based on the percentage ratio $\Delta\mathcal{E}^{10}_{Chu}[\%]$, which is defined as follows,

$$\Delta\mathcal{E}^{10}_{Chu} = \frac{\left(\int_{x_s}^{x_e} E^{10}_{Chu,c}dx - \int_{x_s}^{x_e} E^{10}_{Chu,nc}dx\right)}{\int_{x_s}^{x_e} E^{10}_{Chu,nc}dx}100 \tag{8}$$

Where $E^{10}_{Chu,nc}$ and $E^{10}_{Chu,c}$ are the second Mack mode modal energies for the uncontrolled and controlled case, respectively. The effect of the spanwise wavelength of the control streaks ($\lambda_{z,s} = \lambda_z$) is further investigated, and this is varied from $\lambda_z = 0.9$ to 4.8 (Fig. 6a). It is shown that stabilization up to 60% relative to the baseline (uncontrolled) configuration can be achieved for $\lambda_z = 2.4$. As λ_z is increased from 0.9 to 2.4 the maximum streak amplitude at the end of the computational domain increases by approximately 2%. A further increase in streak wavelength to $\lambda_z = 4.8$ leads to a monotonic increase in streak amplitude, but the stabilization benefit reduces to almost 25%. Analysis of the ratio of streamwise distribution of streak wavelength to the local boundary layer thickness (λ_z/δ_{99}) in figure 6b shows that for this case study a maximum stabilization benefit of the streaks is attainable for $\lambda_z/\delta_{99} \approx 8-10$, while a further increase will lead to a significant performance loss of the control method. To further understand the effectiveness of the method, in the following section larger amplitude disturbances are used to also promote transition to turbulence via deterministic forcing.

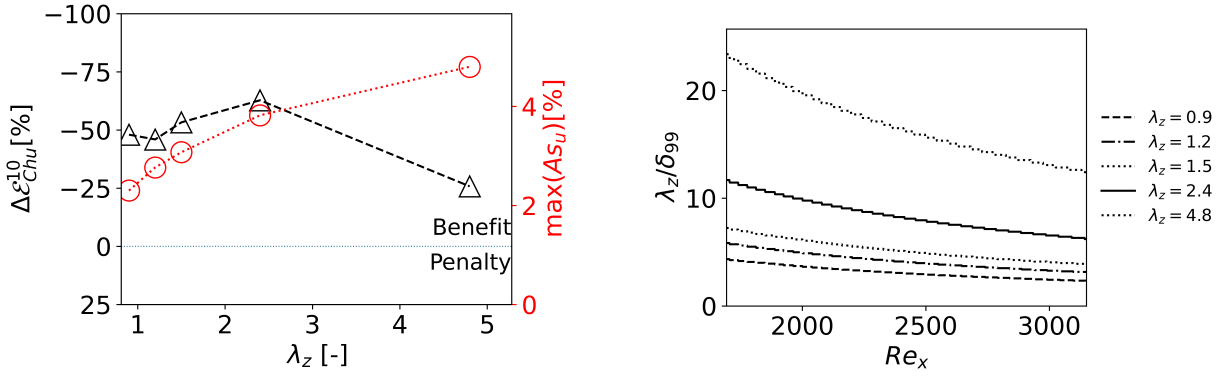

(a) **(b)**

Fig. 6 (*a*) Influence of streak wavelength on second Mack mode stabilization and maximum streak amplitude within the computational domain. (*b*) Streamwise distribution of streaks wavelength to boundary layer thickness ratio.

V. Breakdown to turbulence studies

The results in the previous sections showed that for a Mach 6 configuration the second Mack mode can be successfully stabilized through a spanwise non-uniform surface temperature, with a reduction in the modal energy up to 60%. In this section, the effectiveness of the control method on transition delay is also assessed. In particular, breakdown to turbulence via second Mack mode fundamental resonance is investigated through deterministic forcing. In the following, firstly, a nearly adiabatic flat plate ($T_{w,base} = 6.5$) for $M_\infty = 6$ is investigated and the results are verified with the existing data in the literature. Secondly, a cold wall baseline configuration ($T_{w,b} = 5$) is assessed and the effect of a spanwise non-uniform surface temperature on transition location is determined and quantified.

A. Nearly adiabatic, uncontrolled configuration

The second Mack mode fundamental resonance configuration in Franko and Lele [32] is used as a verification case study to ensure that transition to turbulence can be captured within the computational domain. Tables 1 and 2 summarize operating conditions, computational domain size and grid resolution for this investigation. For time-accuracy, 1200 timesteps per second Mack mode fundamental period ($\tau_0 = 2\pi/\omega_0 \approx 2.6$) are used. After the initial transient (approximately $130\tau_0$), data are acquired for $5\tau_0$ with a sample frequency $f_{Ny} = 12/\tau_0$. This, along with the spanwise resolution of the grid, provides sufficient spectral resolution and range for the frequency (f_n), spanwise wavenumber (k_m) analysis. In the following, f_n and k_m are normalized as $f = f_n\tau_0$ and $k = k_m\frac{\lambda_z}{2\pi}$.

M_∞	$\tilde{T}_\infty$	$T_{w,base}$	$(Re_\infty M_\infty)$	Re_{unit}	Re_{x_s}	Re_{x_e}	$Re_{x_{c,strip}}$	L_{strip}
6.0	65.15K	5	4333	$7.2 \times 10^6$1/m	0	2550	275	5

Table 1 Summary of operating and boundary conditions for the transition to turbulence studies

$[x_s, x_e]$	L_y	λ_z	$N_x \times N_y \times N_z$
[0, 1500]	50	50.27	$2560 \times 150 \times 128$

Table 2 Summary of computational grid details for transition to turbulence studies

Blowing and suction is used to force transition to turbulence and the actuator law for the forcing disturbance introduced in equation 3 is modified as follows,

$$\begin{cases} \frac{\tilde{v})_{wall}}{\tilde{c})_\infty} = v_{wall} = \exp(-\epsilon\xi^2) g(z) \sum_i A_i \sin(\omega_i t - k_i z) \\ g(z) = \left[1.0 + 0.1\left(\exp\left[-\left(\frac{z-2\pi}{2\pi}\right)^2\right] - \exp\left[-\left(\frac{z+2\pi}{2\pi}\right)^2\right]\right)\right] \end{cases} \tag{9}$$

where A_i, ω_i and k_i are the non-dimensional amplitudes, angular frequencies and spanwise wavenumbers of the wall normal disturbances, with values based upon Franko and Lele [32] studies and summarized in table 3. A series of lower amplitude travelling and standing 2D and 3D waves are superimposed to the second Mack mode fundamental disturbance ($\omega_0 = 2.4$) wave to trigger non-linear interactions. The function $g(z)$ in equation 9 introduces spanwise asymmetry and promotes faster transition to turbulence [33]. The center of the actuator is at $x_{c,strip} = 17.5$ and its length $L_{strip} = 5$.

Figure 7 shows the achieved grid resolution in near wall units (indicated with superscript $^+$), along with the skin friction coefficient depicting laminar to turbulence transition. The qualitative comparison in figure 8 of the Mach number distribution at a fixed wall normal distance ($y = 4.5$) with Franko and Lele [32] results shows similar flow topology for the two independent studies. This is a confirmation that transition to turbulence via second Mack mode fundamental resonance has been promoted. The different location of laminar to turbulence transition is likely associated to a mismatch in unit Reynolds number [1] which is not further investigated. For the purpose of these studies that are focused on the assessment of the effect of a spanwise non-uniform surface temperature boundary condition on transition to turbulence via second Mack mode fundamental resonance, the agreement is deemed satisfactory. In the next section the effect of the spanwise non-uniform surface temperature on second Mack mode stabilization, non-linear interactions

Mode (i)	$A_i[\times M_\infty]$	f_i	k_i
0	0.1	1	0
1	0.005	1/2	0
2	0.005	0	[1, 2]
3	0.005	1/2	±1
4	0.005	1	±2
5	0.005	1	±1

Table 3 Summary of the harmonics introduced via blowing and suction to promote transition to turbulence

and transition to turbulence is investigated. A cold flat plate ($T_w/T_{aw} \approx 0.67$) configuration is used as a baseline to avoid exceeding adiabatic conditions when the control method is also enforced.

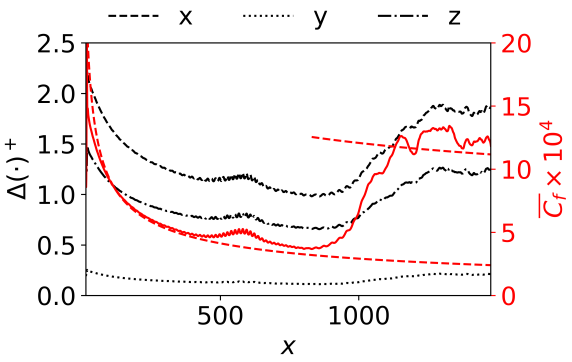

Fig. 7 Time and spanwise averaged DNS grid resolution in near wall units (left y-axis) and skin friction coefficient (right y-axis) for the isothermal (nearly adiabatic) configuration. The red dashed lines indicate the laminar and turbulent (Van Driest II, [34]) correlations.

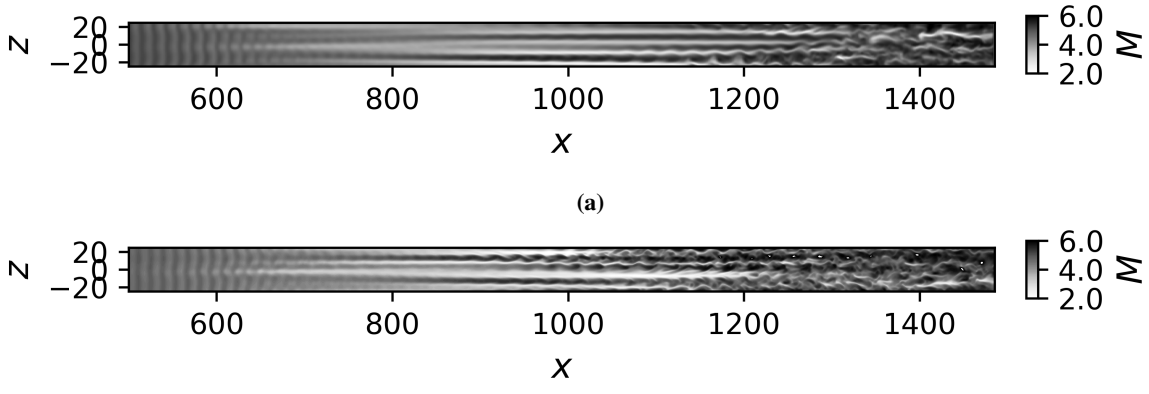

(a)

(b)

Fig. 8 Mach number distribution at $y = 4.5$. (*a*) Figure 18 from Franko and Lele [32] reproduced with permission; (*b*) current study.

B. Cold configuration with and without control

A zero pressure gradient, Mach 6 boundary layer over an isothermal cold ($T_w = 5$, $T_w/T_{aw} \approx 0.67$) wall is studied via DNS, and used as a baseline to assess the effectiveness of the novel control method. The forcing strategy to promote transition to turbulence and the computational details are the same used in the section above (Sec. V.A). A slightly coarser grid resolution is achieved, as a result of the thinner boundary layer due to the colder wall. However, typical DNS grid requirements [32] are met, with Δx^+ and Δz^+ below 3.5 and 2.5, respectively, first cell $y^+ < 0.5$, and approximately 24 points per second Mack mode fundamental streamwise wavelength. The flow topology for the cold, uncontrolled configuration is similar to the nearly adiabatic case introduced in the previous section (Fig. 9a). Downstream of the saturation of the second Mack mode ($x \approx 650$), there is formation of large amplitude steady streaks with the most energetic harmonic being the $(f, k) = (0, 4)$ (Fig. 9b). This is not part of the spectrum of the forcing disturbance law, and it is the result of triadic, difference interaction of the disturbance oblique waves (mode 4 in table 3).

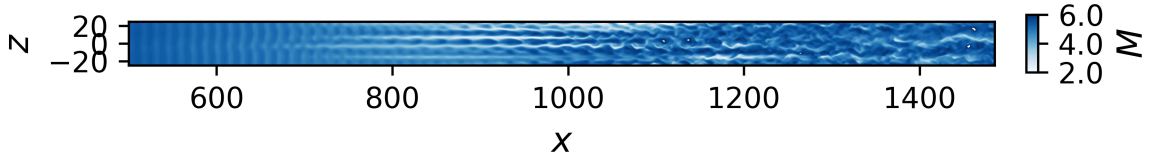

(a)

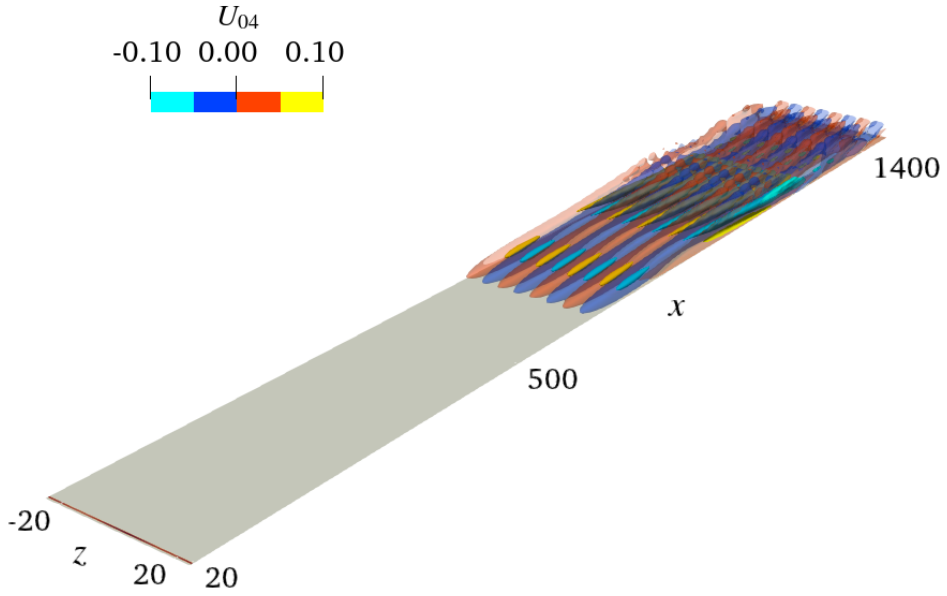

(b)

Fig. 9 (*a*) Mach number distribution at $y = 4.5$ for the uncontrolled, cold wall configuration. (*b*) Isosurfaces of streamwise velocity fluctuations for the most energetic streaks, $(f, k) = (0, 4)$ for the baseline, uncontrolled configuration; figure (*b*) aspect ratio set to 4 for visualization purposes.

For the controlled configuration, a spanwise non-uniform surface temperature with $A_{T_w} = 0.25$ and $k_s = 2\pi/\lambda_{z,s} = 4$ is enforced in the computational domain to understand whether transition delay can be achieved via either constructive or destructive interference of the large amplitude streaks due to non-linear interactions and the control-streaks (Fig. 10). The spanwise variation in surface temperature corresponds to approximately 162K. In addition, the choice of the fundamental wavenumber of the control-streaks (k_s) is based upon the studies presented in section IV.B. This corresponds to a wavelength that is approximately 9 times the boundary layer thickness at the inlet of the computational domain ($\delta_{99,in}$). For this operating conditions, it is expected to provide a near-optimum stabilization of the second Mack mode.

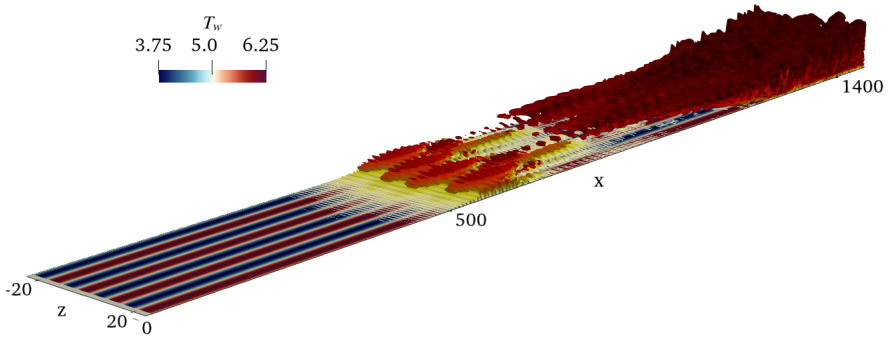

Fig. 10 Transition to turbulence via second Mack mode fundamental resonance for the controlled configuration. $M_\infty = 6$, $Re_{unit} = 7.2 \times 10^6$1/m, $T_{w,base} = 5$, $A_{T_w} = 0.25$, $k_s = 0.3$. Isosurfaces of Q-criterion colored with Mach number, depicting onset of second Mack mode ($x \approx 500$) and transition to turbulence ($x \approx 1000$). Figure aspect ratio set to 4 for visualization purposes.

The spanwise non-uniform surface temperature generates control-streaks with a maximum amplitude of approximately 3.5% of the freestream speed (u_∞). This is quantified through the amplitude of the $(f, k) = (0, 4)$ Fourier harmonic of the streamwise velocity in figure 11a for $x < 500$. Further downstream ($x > 500$), the amplitude of the $(f, k) = (0, 4)$ harmonic rapidly grows, and it peaks at around $x \approx 650$ to approximately 20% (fig. 11a). The comparison with the uncontrolled configuration indicates the presence of constructive interference between the control-streaks and the streaks due to non-linear interactions. The control-streaks stabilize the second Mack mode with a significant reduction in the amplitude of the modal energy of the fundamental, 2D, harmonic, depicted by the $(f, k) = (1, 0)$ harmonic in figure 11b for $x \approx 600$. This is further confirmation of the results presented in section IV relative to the effectiveness of the control method in the stabilization of the second Mack mode, and it demonstrates the appropriate selection of the fundamental wavelength of the streaks for second Mack mode stabilization. It is acknowledged though that a parametric study would be required to further confirm this choice. In the rest of the paper, the skin friction coefficient is further investigated to determine the effect of the control method on transition to turbulence.

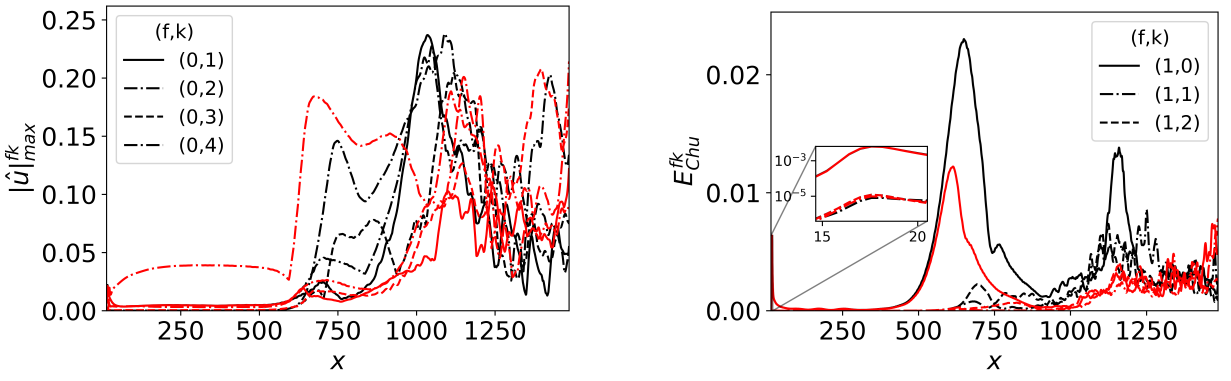

Fig. 11 Streamwise distribution of the amplitude of (*a*) streaks harmonics and (*b*) second Mack mode modal energy. Black lines: uncontrolled configuration; red lines: controlled configuration. The inset in (*b*) depicts the modal energy introduced by the blowing and suction at the second Mack mode fundamental frequency, and it is the same for the uncontrolled and controlled configuration.

Figure 12 shows the instantaneous distribution of skin friction coefficient for both the uncontrolled and controlled configurations. At around $x \approx 700$, the control method significantly reduces the peak value of C_f associated to the high-frequency fluctuations of the second Mack mode. Further downstream, for the controlled configuration, the large amplitude streaks due to non-linear interactions and constructive interference with the control-streaks stay coherent for a longer streamwise distance (Fig. 12). Overall, this indicates a delay in the turbulence breakdown due to the control method. This is further quantified through investigation of the streamwise distribution of the time and spanwise averaged skin friction coefficient ($\overline{C_f}$) in figure 13. For this case study, the streamwise extent of laminar to turbulence transition delay due to the control method is approximately $80\delta_{99,in}$. In addition, a Hilbert transform ($\mathcal{H}(\cdot)$) of the spanwise-averaged skin friction coefficient ($\langle C_f \rangle_z$) is used to quantify the high-frequency (second Mack mode type) peak fluctuations associated with planar waves. At the location of second Mack mode maximum amplification ($300 < x/\delta_{99,in} < 500$, Fig. 13) the analysis indicates that the control method reduces the peak shear-stresses fluctuations and their streamwise extent by approximately 30% and $80\delta_{99,in}$, respectively. It is speculated that this reduction in amplitude and extent of the high-frequency peak stresses could be beneficial for high-cycle fatigue.

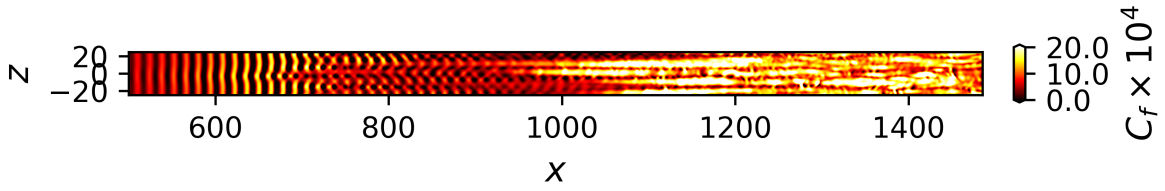

(a)

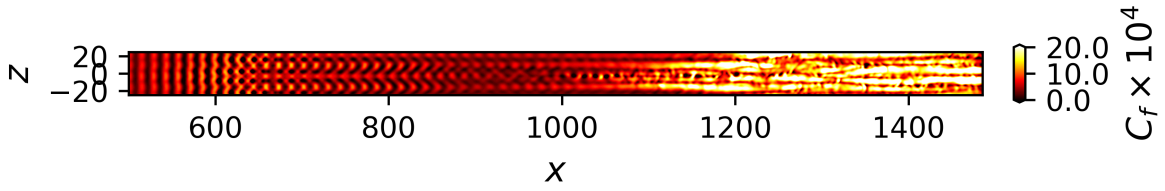

(b)

Fig. 12 Instantaneous snapshots of skin friction coefficient for (*a*) uncontrolled and (*b*) controlled configuration.

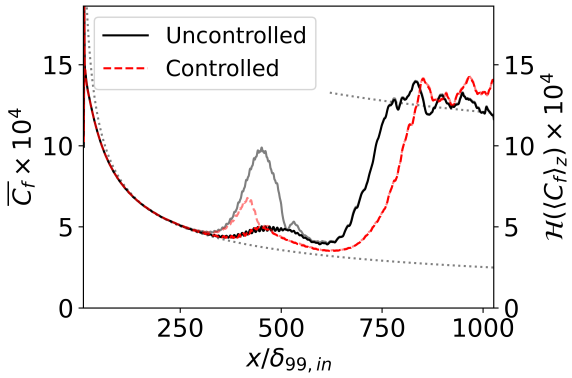

Fig. 13 Effect of control method on streamwise distribution of time and spanwise averaged skin friction coefficient (left y-axis). Grey dotted lines indicate the laminar and turbulent correlations; x-axis scaled with boundary layer thickness at the inlet of the computational domain ($\delta_{99,in}$). The shaded solid black and dashed red lines refer to the right y-axis, which indicates the Hilbert transform of the spanwise-averaged skin friction coefficient.

The isentropic efficiency of the control method is evaluated relative to a fully laminar configuration with a uniform

$T_w = 5$, which represents the notional, optimal solution. The efficiency is quantified with the entropy function (ζ), which is defined as follows,

$$\zeta = \frac{1}{L_y \lambda_z} \int \int \exp\left[\frac{-(\tilde{s} - \tilde{s}_\infty)}{\tilde{R}_{gas}}\right] dydz \tag{10}$$

where $\tilde{R}_{gas}$ is the gas constant, s is the local entropy, and s_∞ is evaluated based on the freestream temperature and pressure. The control method delays the efficiency losses due to transition to turbulence further downstream, but the overall efficiency benefit at the end of the computational domain remains marginal (Fig. 14) compared to a fully laminar configuration. Optimization strategies should be investigated to enhance the performance of the control method, which is promising and with several potential aero-thermal-structural implication benefits.

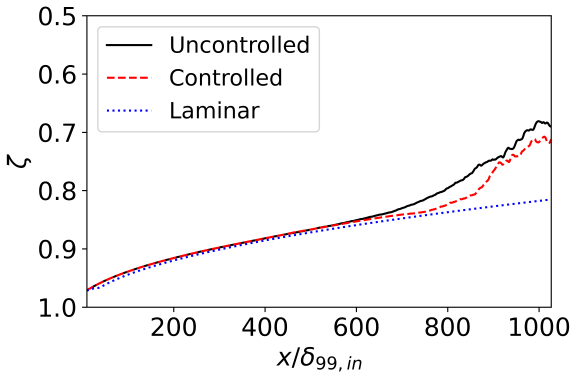

Fig. 14 Effect of control method on streamwise distribution of integrated entropy function.

VI. Conclusions

The novel contribution of this work is the computational assessment of the effectiveness of a novel control method that generates streaks through manipulation of the surface temperature to stabilize second Mack mode and delay transition to turbulence. For a Mach 6, zero pressure gradient, flat plate configuration at flight representative conditions, it is shown that second Mack mode can be stabilized via streaks generated through a spanwise non-uniform surface temperature, and near-optimum performance are achieved for a wavelength of the control-streaks approximately 8 to 10 times the boundary layer thickness in the region of second Mack mode onset, saturation and decay.

Breakdown to turbulence via deterministic forcing is also investigated, and for the second Mack mode fundamental resonance scenario it is shown that the control-streaks stabilize the second Mack mode, reduce the high-frequency (second Mack mode related) peaks in the skin friction coefficient and ultimately delay transition. Overall, this work provides initial guidance for further experimental and numerical investigations of the novel control method, which could enhance the aero-thermal-structural efficiency of future hypersonic technologies.

Acknowledgments

The authors gratefully acknowledge the financial support of Dstl through the WSRF program (task number 0105), and EPSRC for the computational time made available on the UK supercomputing facility ARCHER2 via the UK Turbulence Consortium (EP/R029326/1).

A. Spanwise grid refinement studies

The influence of the number of nodes per fundamental spanwise wavelength (n_z) of the streaks on streaks amplitude and second Mack mode amplification is investigated. Three grid refinement levels are used with $n_z = 13$, 45 and 75, and these are named 1, 2 and 3, respectively (table 4). The finest grid level is based upon previous grid convergence studies for the assessment of the hypersonic boundary layer transition with surface roughness [35]. Overall, for the

three grid levels the maximum amplitude of the streaks and of the linear amplification of the second Mack mode modal energy is within approximately 0.8% and 5%, respectively.

Grid level	No. nodes ($n_x \times n_y \times n_z$)	λ_z	$T_{w,base}$	A_{T_w}
1	$1200 \times 211 \times 13$	1.2	3.6	0.3
2	$1200 \times 211 \times 45$	1.2	3.6	0.3
3	$1200 \times 211 \times 75$	1.2	3.6	0.3

Table 4 Summary of the spanwise grid refinement studies; $M_\infty = 4.8$**,** $(Re_\infty M_\infty) = 1.0\times10^5$**,** $\tilde{h}_{0,\infty} = 0.3\times10^6$**J/kg.**

B. Benchmark of current LST results

The linear stability theory (LST) code used within this study is benchmarked with previous data in the literature [3]. The effect of Mach number on maximum spatial growth rate (Fig. 15) is assessed at a fixed freestream specific total enthalpy ($\tilde{h}_{0,\infty} \approx 0.31 \times 10^6$ J/kg). The analysis was carried out at a fixed Re_x (= 1500) and by varying the non-dimensional frequency ($F = \omega/Re_x$) of the perturbation. Overall, the agreement in maximum spatial growth rate for the second Mack mode was deemed satisfactory for the purpose of this work.

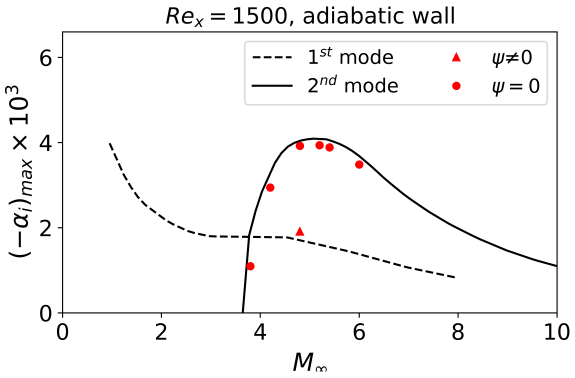

Fig. 15 Effect of Mach number on maximum spatial growth rate of first and second Mack mode instability within the laminar (self-similar) boundary layer over an adiabatic flat plate for $Re_x = 1500$**. Red markers represent the current study; solid and dashed lines are reproduced from Mack (1975) [3].**

References

[1] Anderson, J. D., *Hypersonic and high temperature gas dynamics*, AIAA, 1989. https://doi.org/https://doi.org/10.2514/4.861956.

[2] Laurence, S. J., Wagner, A., and Hannemann, K., "Experimental study of second-mode instability growth and breakdown in a hypersonic boundary layer using high-speed schlieren visualization," *J. Fluid Mech.*, Vol. 797, 2016, pp. 471–503. https://doi.org/10.1017/jfm.2016.280.

[3] Mack, L. M., "Linear stability theory and the problem of supersonic boundary-layer transition," *AIAA J.*, Vol. 13, 1975, pp. 278–289. https://doi.org/10.2514/3.49693.

[4] Zhu, Y., Chen, X., Wu, J., Chen, S., Lee, C., and Gad-El-Hak, M., "Aerodynamic heating in transitional hypersonic boundary layers: Role of second-mode instability," *Phys. Fluids*, Vol. 30, 2018. https://doi.org/10.1063/1.5005529.

[5] Paredes, P., Choudhari, M. M., and Li, F., "Transition due to streamwise streaks in a supersonic flat plate boundary layer," *Phys. Rev. Fluids*, Vol. 1, 2016. https://doi.org/10.1103/PhysRevFluids.1.083601.

[6] Paredes, P., Choudhari, M. M., and Li, F., "Instability wave-streak interactions in a supersonic boundary layer," *J. Fluid Mech.*, Vol. 831, 2017, pp. 524–553. https://doi.org/10.1017/jfm.2017.630.

[7] Sharma, S., Shadloo, M. S., Hadjadj, A., and Kloker, M. J., "Control of oblique-type breakdown in a supersonic boundary layer employing streaks," *J. Fluid Mech.*, Vol. 873, 2019, p. 1072–1089. https://doi.org/10.1017/jfm.2019.435.

[8] Kneer, S., Guo, Z., and Kloker, M. J., "Control of laminar breakdown in a supersonic boundary layer employing streaks," *J. Fluid Mech.*, Vol. 932, 2022, p. A53. https://doi.org/10.1017/jfm.2021.1047.

[9] Celep, M., Hadjadj, A., Shadloo, M. S., Sharma, S., Yildiz, M., and Kloker, M. J., "Effect of streak employing control of oblique-breakdown in a supersonic boundary layer with weak wall heating/cooling," *Phys. Rev. Fluids*, Vol. 7, 2022, p. 053904. https://doi.org/10.1103/PhysRevFluids.7.053904, URL https://link.aps.org/doi/10.1103/PhysRevFluids.7.053904.

[10] Zhou, T., Lu, Y., Liu, Z., and Yan, C., "Controlling second-mode oblique breakdown in high-speed boundary layers using streak: A direct numerical simulation study," *Phys. Fluids*, Vol. 35, No. 8, 2023, p. 084102. https://doi.org/10.1063/5.0159639.

[11] Andersson, P., Brandt, L., Bottaro, A., and Henningson, D. S., "On the breakdown of boundary layer streaks," *J. Fluid Mech.*, Vol. 428, 2001, pp. 29–60. https://doi.org/10.1017/S0022112000002421.

[12] Hanifi, A., Schmid, P. J., and Henningson, D. S., "Transient growth in compressible boundary layer flow," *Phys. of Fluids*, Vol. 8, No. 3, 1996, pp. 826–837. https://doi.org/10.1063/1.868864.

[13] Tumin, A., and Reshotko, E., "Optimal Disturbances in Compressible Boundary Layers," *AIAA J.*, Vol. 41, No. 12, 2003, pp. 2357–2363. https://doi.org/10.2514/2.6860.

[14] Caillaud, C., Lehnasch, G., Martini, E., and Jordan, P., "Effect of streaks on hypersonic boundary layer instability," 2023. URL http://arxiv.org/abs/2311.02463.

[15] Marxen, O., Iaccarino, G., and Shaqfeh, E. S., "Disturbance evolution in a Mach 4.8 boundary layer with two-dimensional roughness-induced separation and shock," *J. Fluid Mech.*, Vol. 648, 2010, pp. 435–469. https://doi.org/10.1017/S0022112009992758.

[16] Fong, K. D., Wang, X., Huang, Y., Zhong, X., McKiernan, G. R., Fisher, R. A., and Schneider, S. P., "Second mode suppression in hypersonic boundary layer by roughness: Design and experiments," *AIAA J.*, Vol. 53, 2015, pp. 3138–3143. https://doi.org/10.2514/1.J054100.

[17] Taylor, O. W., and Bruce, P. J., "A parametric study into the effects of surface roughness spacing on the transition of hypersonic boundary layers," 54th AIAA Aerospace Sciences Meeting, 2016. https://doi.org/10.2514/6.2016-1125.

[18] Paredes, P., Choudhari, M. M., and Li, F., "Instability wave-streak interactions in a high Mach number boundary layer at flight conditions," *J. Fluid Mech.*, Vol. 858, 2019, pp. 474–499. https://doi.org/10.1017/jfm.2018.744.

[19] Duan, L., Wang, X., and Zhong, X., "Stabilization of a Mach 5.92 Boundary Layer by Two-Dimensional Finite-Height Roughness," *AIAA J.*, Vol. 51, No. 1, 2013, pp. 266–270. https://doi.org/10.2514/1.J051643.

[20] Ozawa, K., Xia, C., Rigas, G., and Bruce, P. J., "Passive control of high-speed boundary layer transition using non-uniform surface temperature distributions," AIAA SCITECH 2023 Forum, 2023. https://doi.org/10.2514/6.2023-0849.

[21] Ozawa, K., Bruce, P. J., and Rigas, G., "Measurement of streaks generated by non-uniform surface temperature distributions for delaying high-speed boundary layer transition," 58th 3AF International Conference on Applied Aerodynamics, Orleans, France, 2024.

[22] Bitter, N. P., and Shepherd, J. E., "Stability of highly cooled hypervelocity boundary layers," *J. Fluid Mech.*, Vol. 778, 2015, pp. 586–620. https://doi.org/10.1017/jfm.2015.358.

[23] Nagarajan, S., Lele, S. K., and Ferziger, J. H., "A robust high-order compact method for large eddy simulation," *J. Comp. Phys.*, Vol. 191, No. 2, 2003, pp. 392–419.

[24] Nagarajan, S., Lele, S., and Ferziger, J., "Leading-edge effects in bypass transition," *J. Fluid Mech.*, Vol. 572, 2007, pp. 471–504.

[25] Ma, Y., and Zhong, X., "Receptivity of a supersonic boundary layer over a flat plate. Part 2. Receptivity to free-stream sound," *J. Fluid Mech.*, Vol. 488, 2003, pp. 79–121. https://doi.org/10.1017/S0022112003004798.

[26] Pagella, A., Rist, U., and Wagner, S., "Numerical investigations of small-amplitude disturbances in a boundary layer with impinging shock wave at Ma=4.8," *Phys. of Fluids*, Vol. 14, 2002, pp. 2088–2101. https://doi.org/10.1063/1.1480265.

[27] Egorov, I. V., Fedorov, A. V., and Soudakov, V. G., "Direct numerical simulation of disturbances generated by periodic suction-blowing in a hypersonic boundary layer," *Theor. Comp. Fluid Dyn.*, Vol. 20, 2006, pp. 41–54. https://doi.org/10.1007/s00162-005-0001-y.

[28] Unnikrishnan, S., and Gaitonde, D. V., "Linear, nonlinear and transitional regimes of second-mode instability," *J. Fluid Mech.*, Vol. 905, 2020. https://doi.org/10.1017/jfm.2020.781.

[29] Mack, L. M., "A numerical study of the temporal eigenvalue spectrum of the Blasius boundary layer," *J. Fluid Mech.*, Vol. 73, 1976, pp. 497–520. https://doi.org/10.1017/S002211207600147X.

[30] Chu, B.-T., "On the energy transfer to small disturbances in fluid flow (Part I)," *Acta Mech.*, Vol. 1, No. 3, 1965, pp. 215–234.

[31] Schneider, S. P., "Flight data for boundary-layer transition at hypersonic and supersonic speeds," *J. Spacecraft Rockets*, Vol. 36, No. 1, 1999, pp. 8–20.

[32] Franko, K. J., and Lele, S. K., "Breakdown mechanisms and heat transfer overshoot in hypersonic zero pressure gradient boundary layers," *J. Fluid Mech.*, Vol. 730, 2013, pp. 491–532.

[33] Wang, M., Lele, S. K., and Moin, P., "Sound radiation during local laminar breakdown in a low-Mach-number boundary layer," *J. Fluid Mech.*, Vol. 319, 1996, p. 197–218. https://doi.org/10.1017/S0022112096007318.

[34] Bradshaw, P., "Compressible turbulent shear layers," *Annu. Rev. Fluid Mech.*, Vol. 9, 1977, pp. 33–52. https://doi.org/10.1146/annurev.fl.09.010177.000341.

[35] Lefieux, J., Garnier, E., and Sandham, N., "DNS study of roughness-induced transition at Mach 6," *AIAA Aviation 2019 Forum*, 2019, p. 3082. https://doi.org/10.2514/6.2019-3082.